# Exploring the Rehydroxylation Reaction of Pyrophyllite by Ab Initio Molecular Dynamics

**Esther Molina-Montes,[†] Davide Donadio,[‡] Alfonso Hernández-Laguna,[|] and C. Ignacio Sainz-D´ıaz*,[|]**

*CIBER Epidemiolog´ıa y Salud Pu´blica, Escuela Andaluza de Salud Pu´blica, Campus Uni*V*ersitario de Cartuja, Cuesta del Obser*V*atorio 4, 18080-Granada, Spain, Department of Chemistry, Uni*V*ersity of California Da*V*is, One Shields A*V*enue, Da*V*is, CA 95616, and Instituto Andaluz de Ciencias de la Tierra, CSIC/Uni*V*ersidad de Granada, A*V*enida Fuentenue*V*a s/n, 18002-Granada, Spain*

We have investigated the process of rehydroxylation of pyrophyllite as a limiting factor to the dehydroxylation upon thermal treatment. Car-Parrinello molecular dynamics simulations based on density functional theory have been used along with the metadynamics algorithm. Two possible rehydroxylation mechanisms reaction have been characterized, related to two possible intermediate structures along the rehydroxylation paths, and both involve the interaction of the apical oxygen atoms. At high temperature, the rehydroxylation reaction is highly competitive (free energy barrier ($\Delta F$) ) 1.5 kcal/mol) and inhibits the progress of the dehydroxylation reaction ($\Delta F$ ) 40 kcal/mol). In addition to the rehydroxylation of the dehydroxylated structure, the water molecule supports the interconversion of the cross and on-site intermediates as well. Thus, rehydroxylation and interconversion among intermediates can justify the wide range of transformations as a function of the temperature observed experimentally.

## Introduction

Pyrophyllite is a dioctahedral 2:1 phyllosilicate in which a sheet of octahedrally coordinated aluminum cations (octahedral sheet) is sandwiched between two sheets of corner sharing silica tetrahedra. In the octahedral sheet, two-thirds of the available octahedral sites are occupied by aluminum atoms and one-third is vacant. The occupied octahedra show a quasi hexagonal symmetry around the vacant octahedron. Two adjacent octahedra are linked by hydroxyl groups. It is a mineral widely used in the manufacture of glass, ceramics, refractory materials, and pressure-transfer media. In many of these processes, some dehydration and dehydroxylation processes are produced at high temperature. A failure in the stability under thermal treatment of this mineral can produce a change in the physical-chemical properties, due to the dehydroxylation process, rehydration, and other mineral transformations. A better knowledge of this thermally induced degradation can be very useful to understand the general behavior of this class of clay minerals upon thermal treatment and for industrial applications.

The dehydroxylation reaction consists of the loss of hydroxyl groups from their combination in the octahedral sheet into a water molecule that eventually migrates from the octahedral hole into the interlaminar space and diffuses throughout the interlayer region. The final dehydroxylated structure of pyrophyllite consists of 5-fold coordinated, distorted, trigonal bipyramidal $AlO_5$ units joined by a residual oxygen ($O_r$) in the octahedral sheet (Figure 1), sandwiched between two distorted but intact tetrahedral $SiO_4$ sheets.[1,2] This reaction occurs over a broad range of temperatures from 400 to 850 °C. Furthermore the dehydroxylated pyrophyllite can be rehydroxylated when the temperature remains under the critical temperature of amorphization and upon cooling in the presence of water,[3] recovering


**Figure 1.** Dehydroxylation and rehydroxylation processes in pyrophyllite (crystal structures are viewed from the 001 plane). The OH groups involved in the cross and on-site mechanisms are shown. H, Al, Si, and O atoms are in black, pink, gray, and red colors, respectively. The Al, O, and H atoms involved in the reactions are highlighted as balls.

the initial structure of pyrophyllite (Figure 1) through the reaction: $O_r + H_2O$ 1 2(OH). However, at high temperatures the water molecules are released but with some difficulties owing to kinetics aspects and heterogeneous temperature distribution. In fact, the dehydroxylation reaction is assumed to be actually a combination of dehydroxylation and rehydroxylation processes.[4] By means of IR spectroscopy, the temperature dependence of the stretching frequencies of the OH bonds was probed during the dehydroxylation process,[5] so as to determine the temperature evolution of the reaction by differential thermal analysis (DTA).[6] Changes in crystal lattice structure were detected by X-ray diffraction,[7] and the kinetics of this process was investigated.[8,9] However, the low crystalline grade, the high degree of disorder, and the high dispersion in particle size hampered a clear interpretation of experiments. For this reason, subjects such as the reaction mechanism and the broad range of temperature behavior are still not well understood.

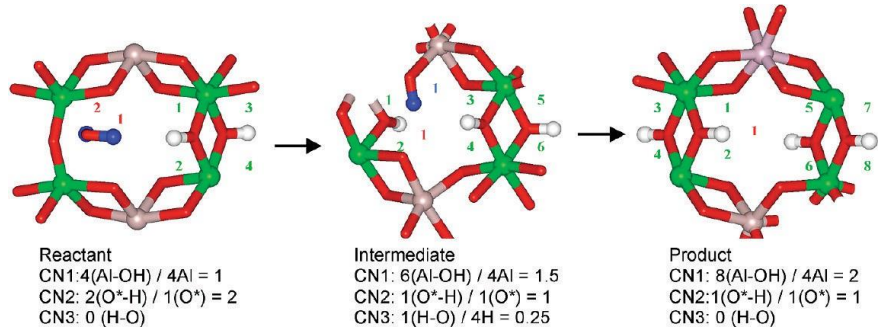


**Figure 2.** Definition of the three coordination numbers CN chosen as collective variables (CV) along the reaction path. H, Al, and O atoms are in white, pink, and red colors, respectively; in the water molecule the H atoms are in blue color. The Al atoms used in the CV definition are highlighted in green color. The O* means the oxygen of the water molecule.

Recently, quantum mechanics has been applied to the study of dehydroxylation of pyrophyllite to support the interpretation of some of these phenomena at the atomic scale. From these calculations, the energetic of the dehydroxylation reaction was accurately determined,[10-14] finding that such reaction goes at least throughout two competitive mechanisms (Figure 1), (i) an "on-site" mechanism evolving the bridging hydroxyl groups of an octahedral pair; and (ii) a "cross" mechanism where two hydroxyl groups react across the dioctahedral vacancy. The free energy barrier is lower for the latter mechanism at high temperature (>900 K). In both cases, the first step of the reaction generates intermediates, the cross and on-site semidehydroxylates. A variant of these mechanisms at high temperature involves the assistance of the apical oxygens.[12] The existence of intermediates during the reaction was proposed in several experimental[4,5,15] and theoretical studies.[10,11,13]

In this work, we aim at investigating the rehydroxylation reaction mechanisms starting from the semidehydroxylate products from the previous dehydroxylation reaction.[12,13] We find that the rehydroxylation reaction inhibits the progress of dehydroxylation and the presence of water facilitates the interconversion of intermediates. These results justify the wide range of behaviors as a function of temperature observed experimentally for the dehydroxylation of phyllosilicates.

## Methods

We perform ab initio Car-Parrinello molecular dynamics[16] (MD) simulations, based on the density functional theory (DFT) utilizing the CPMD package v.3.9,[17] in the NVE ensemble. We use the generalized gradient approximation (GGA) with the BLYP parametrization[18,19] for the exchange and correlation functional along with norm-conserving pseudopotentials in the Troullier-Martins form.[20] A plane-wave basis set with energy cutoff of 70 Ry was used for describing the wave functions of the valence states. Although this standard approach has proven useful for exploring complex processes in solid state,[25,26] in our system, pyrophyllite (crystallographic data obtained from Wardle & Brindley[23]), a standard MD simulation would require an unfeasibly long run to explore the complex processes of dehydroxylation and rehydroxylation. Therefore we exploit the so-called metadynamics method[24,25] to achieve an efficient exploration of these complex processes in condensed phases and get a rough estimate of the free energy profiles in a coarse grained space defined by a set of collective variables (CV). In our previous work, this procedure has proven efficient for studying the dehydroxylation reaction.[12] CVs are generally analytical functions of the atomic coordinates. In this work, we choose interatomic distances (D) and coordination numbers (CN), which are defined by means of sums of rational functions. More details on the construction and use of such CVs are given elsewhere.[12,25-27]

We performed MD simulations on the semidehydroxylate products of both the on-site and cross mechanisms with a time step of 0.12 fs and fictitious electron mass of 800 au at constant volume and temperature. Before switching on the metadynamics, the system is equilibrated at the temperature of interest for 1.6 ps by rescaling the velocities to the target temperature. During the equilibration runs no chemical reaction was observed.

A detailed explanation of metadynamics CVs design applied to the study of the dehydroxylation reaction can be found in our previous work.[12] We specifically defined the following CVs for the study of the rehydroxylation reaction on the semidehydroxylate derivatives with water, D1 (distance between the H and O atoms across the octahedral vacancy), D2 (distance between the H and O nonbonded atoms of the same $Al(OH)_2Al$ site), CN1 (coordination number of Al with the OH groups), CN2 (coordination of the O atom of the water molecule with all H atoms that form the OH groups; this O atom is different for the on-site and cross mechanisms), and CN3 (coordination of the apical O atoms with the H atoms). The value of these CVs varies along the reaction path so that the intermediate and product states could be easily recognized and followed (Figure 2).

The details of the free energy calculations within the metadynamics scheme is reported extensively elsewhere.[27,30,31] Summarizing, the metadynamics methods consists of coupling the microscopic system described by MD to a suitably defined coarse-grained space of CVs (s), which is biased by a history-dependent potential ($V_G(s,t)$). $V_G(s,t)$ is made of a sum of Gaussians centered on the trajectory of the CVs with a chosen width and height. After a sufficiently long time, this potential provides an estimate of the underlying free energy surface in the space of the CVs

$$\lim_{t\to\infty} V_G(s,t) \approx F(s)$$

The biasing potential helps to overcome the local minima of the free energy surface (FES), forcing the system to explore the relevant parts of the coarse grained space defined by the CVs. The sum of the Gaussians provides an estimation of the FES with an accuracy that depends on the dimensionality of the CV space, their diffusion coefficient and the parameters of the history dependent potential.[27] Spherical Gaussian hills with a fixed height of about 1.25 kcal/mol are added approximately every 10 fs. The widths of the Gaussians were set to 0.01-0.02

at 900 K and to 0.02-0.03 at 1500 K. These values for the width are chosen as one-fifth of the amplitude of the fluctuations of the related CV at the equilibrium, and the height is much smaller than the potential energy barriers estimated for the dehydroxylation reaction both theoretically[10,12] and experimentally.[28] Finally, the parameters of the Gaussians that form the history-dependent potential have been chosen, so to reproduce the FES with an accuracy of ~2 kcal/mol.

In both mechanisms of dehydroxylation process, one O-H bond is broken and, at the same time, a nonbonding H...O distance changes provoking this O-H bond breaking. Then, only one CV, D1, or D2, can be enough to explore the formation of the water molecule. Nevertheless, we include both CVs to explore both mechanisms simultaneously, avoiding any forced bias to any mechanism. Besides, we can observe the competition between both mechanisms with this approach. During the simulation, we observe the reaction path through the lowest free energy barrier by means of the free energy surface (FES) profile. To explore the possible existence of other mechanisms we performed new simulations increasing the width of the Gaussians associated to the CV related to the other mechanism. This allows us to explore the other reaction-path without altering the energy profile of the other path. This procedure can be extended to other CVs.

When the dynamical reaction trajectories were identified, we explored the topology of the FES, where we identified the critical points (minima and transition states) and characterized them by means of static quantum-mechanical calculations at 0 K. The transition states were optimized by the PRFO algorithm[29] and the reaction coordinates were confirmed by searching for the negative eigenvalues of the dynamical matrix. The activation energy is the potential energy barrier, calculated at 0 K, that one structure of minimal energy has to overcome through a transition state to form the another structure of minimal energy.

## Results

**Rehydroxylation of the Semidehydroxylate Intermediates.** ***Direct Rehydroxylation Paths.*** The first step of the dehydroxylation reaction is the production of a first water molecule per unit cell, a semidehydroxylate derivative is yielded with the water molecule in the tetrahedral cavity.[12] Direct rehydroxylation mechanisms are achieved by reversing the direct dehydroxylation paths previously studied, yielding similar free energy profiles as those reported previously.[12] For example, starting from the semidehydroxylate intermediate product coming from the cross mechanism with CN1 and CN2 as CVs, the rehydroxylation was found to follow the reverse path as the previous dehydroxylation with an estimated $\Delta F$ of 10.9 kcal/mol at 900 K, that is significantly lower than that of the dehydroxylation ($\Delta F$ ) 48.3 kcal/mol). The total energy profile of such process at 0 K is shown in Figure 3, where the activation energy is 11.05 kcal/mol that is much lower than one of the dehydroxylation way (58.8 kcal/mol). In this semidehydroxylate cross intermediate, the AlAl pairs are partially dehydroxylated remaining alternately AlO(OH)Al and Al(OH)Al groups. During the rehydroxylation the residual oxygens of the AlO(OH)Al groups are protonated from the water molecule, whereas the remaining water OH group reacts with the Al(OH)Al pair yielding the $Al(OH)_2Al$ groups of the pyrophyllite.

From the on-site hydrated semidehydroxylate derivative, we obtained a free energy barrier ($\Delta F$) of 13.1 kcal/mol for the rehydroxylation path throughout the free energy surface (FES) of the dynamics at 900 K (Figure 4). This $\Delta F$ is similar to the cross path and also much lower than that of the on-site

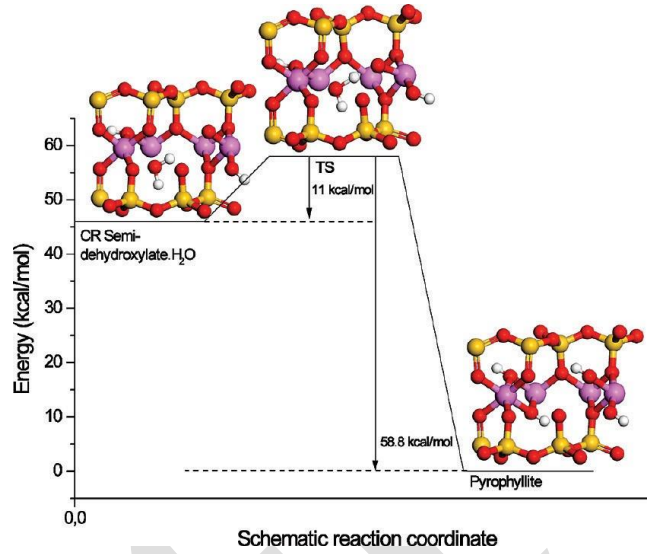


**Figure 3.** Reaction pathway at 0 K of the rehydroxylation of the hydrated crosssemidehydroxylate intermediate through the direct mechanism. H, Al, Si, and O atoms are in white, pink, yellow and red colors, respectively.

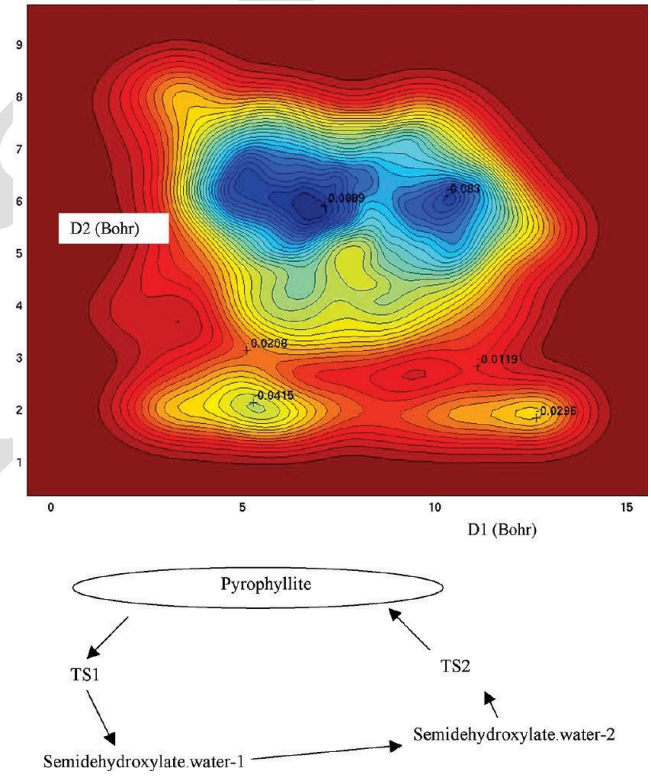


**Figure 4.** Free-energy surface of the dehydroxylation-rehydroxylation of pyrophyllite at 900 K using D1 and D2 as CVs through the direct on-site mechanism. Free energy (Hartrees) varies from dark red at the maximum energy onto blue at the minimum energy.

dehydroxylation path ($\Delta F$ ) 49.9 kcal/mol). We observe four minima and four saddle points in the FES along this reaction path. The two most stable minima (in blue color) correspond to local minima of pyrophyllite with the high fluctuation of the D1 variable (large surface of the blue color). The second minimum of pyrophyllite is only a slightly less stable (about 3.7 kcal/mol) than the most stable one with a low free energy barrier and corresponds to one state of the bending-out-of -plane vibration mode of the OH group, $\gamma$(OH), where the OH groups are oriented toward the interlayer space increasing the D1

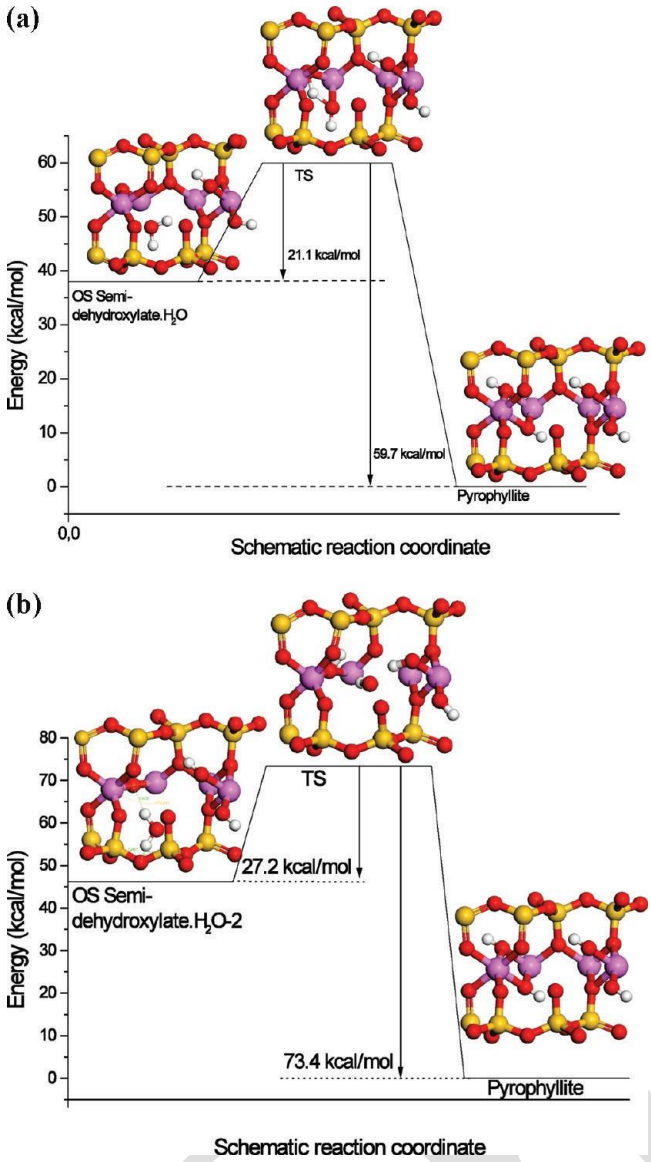


**Figure 5.** Reaction pathway at 0 K of the direct on-site mechanism of the rehydroxylation through the initial semidehydroxylate (a) and the second minimum of semihydroxylate (b), including the critical points of the potential energy surface observed in Figure 4. H, Al, Si, and O atoms are in white, pink, yellow, and red colors, respectively.

distance. The other two minima are involved actually in the reaction paths. One (in green color) corresponds to the on-site semidehydroxylate intermediate where Al-Al pairs are dehydroxylated and not dehydroxylated alternately and the water molecule is trapped in the tetrahedral cavity.[13] Along the rehydroxylation path, we detected one TS that is similar to the TS previously detected in the dehydroxylation.[12] This rehydroxylation path has an activation energy of 21.1 kcal/mol (Figure 5a) that is significantly lower than that of the dehydroxylation path (59.7 kcal/mol). The other secondary minimum is detected (in yellow color) with a similar D2 value to the semidehydroxylate one but with a higher D1 value due to a rotation of the water molecule where the H atoms are oriented toward the bridging residual O atom and the basal tetrahedral oxygens forming a strong H bond (d(H...O) ) 1.628 Å) with the residual O atom increasing the AlOrAl angle (174.8°), and the water O atom is oriented toward the OH group of the vicinal $Al(OH)_2Al$ group (Figure 5b). This minimum is 7.67 kcal/mol less stable than the previous semidehydroxylate one. Nevertheless we detected a saddle point (TS) in the reaction path between this secondary minimum of the semidehydroxylate and the pyrophyllite (Figure 5b), where the residual O atom is protonated and the OH group from the remaining water molecule is stabilized by hydrogen bonds with the surrounding oxygens and with the H atom of the vicinal $Al(OH)_2Al$ group. Crossing this TS to pyrophyllite, the rehydroxylation is produced with an activation energy of 27.2 kcal/mol at 0 K (Figure 5b), which is higher than that of the cross path. This path was not found in the dehydroxylation way probably owing to its activation energy (73.4 kcal/mol) that is higher than that of the direct on-site dehydroxylation way previously reported (59.7 kcal/mol). Nevertheless, the activation energy of this rehydroxylation path is again lower than the dehydroxylation way.

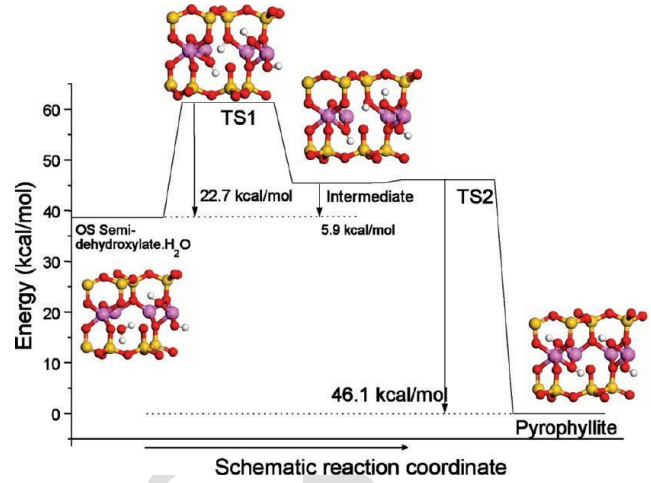


**Figure 6.** Reaction pathway at 0 K of the on-site rehydroxylation mechanism assisted by the apical oxygens. H, Al, Si, and O atoms are in white, pink, yellow, and red colors, respectively.

At 1500 K (using CN1, CN2, and CN3 as CV) we observed the direct on-site rehydroxylation mechanism. After approximately 2500 metadynamics steps, the rehydroxylation occurred. The FES displays a simple double-well profile and we estimate an activation free energy of 7.4 kcal/mol. This $\Delta F$ is much lower than that of the dehydroxylation path ($\Delta F$ ) 52.4 kcal/mol, also using CN1, CN2, and CN3 as CV).[12] The optimization of the critical points on the FES reveals similar structures as those of our previous dehydroxylation simulations[12] and an activation energy of 21.11 kcal/mol at 0 K (Figure 5a), which is lower again than that of the dehydroxylation path (59.7 kcal/mol).[12]

***Rehydroxylation Paths InWolWing Apical Oxygens.*** Starting from the on-site semidehydroxylate derivative with water, we performed simulations using CN1 and CN2 as CVs for the metadynamics at 900 and 1500 K. We found that the rehydroxylation can be mediated by the interaction with the apical oxygens, as in the case of dehydroxylation.[12] The same mechanism involving apical oxygens is observed at 900 and 1500 K, starting from the on-site semidehydroxylate intermediate (Figure 6). The activation free energy of the first step was 19.3 and 10.7 kcal/mol at 900 and 1500 K, respectively. Optimizing the critical points of the reaction path at 0 K, we observe that the activation energy, $E_{act}$, of the protonation of apical O atom was 22.7 kcal/mol while the second step, that is, the deprotonation of the silanol group to protonate the Or atom yielding the pyrophyllite, is spontaneous at low temperature, as no transition state was found in the potential energy surface. The rehydroxylation path ($E_{act}$ ) 22.7 kcal/mol) is more favorable than the dehydroxylation process ($E_{act}$ ) 61.3 kcal/mol in the profile of Figure 6 and 77.8 kcal/mol previously

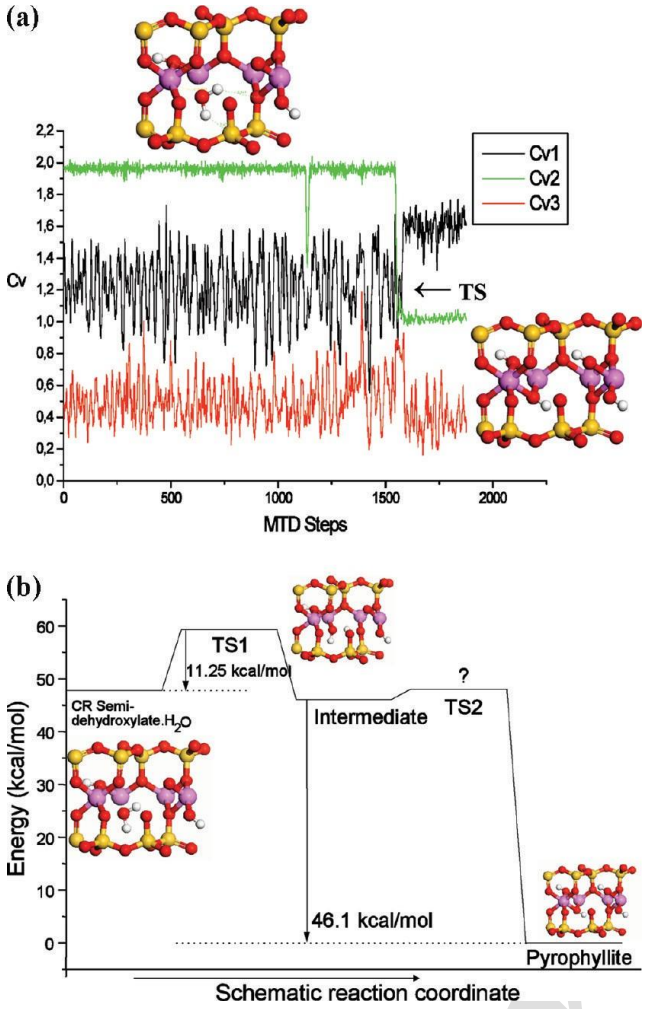


**Figure 7.** Simulation of the rehydroxylation of the cross semidehydroxylate assisted by apical oxygens. (a) Fluctuations the CVs (Cv1, Cv2, and Cv3 correspond to CN1, CN2, and CN3, respectively) along the metadynamics simulation (only the structures of reactant and product are included and the formation of the TS is indicated by a black arrow). (b) Reaction pathway at 0 K. H, Al, Si, and O atoms are in white, pink, yellow, and red colors, respectively.

reported)[12] for this mechanism with the assistance of apical oxygens. In our simulations, we did not find the dehydroxylation path, probably due to its high $E_{act}$, and the direct-dehydroxylation way was observed.[12] Nevertheless, the structure of the intermediates and transition states are similar in both ways and only some differences in the bonds of the AlOH groups are detected (Figure 6).[13] The protonation of the apical oxygens, that is, the presence of silanol groups at high temperature, have been confirmed experimentally by infrared spectroscopy,[15] and theoretically by quantum mechanical calculations.[13]

The rehydroxylation reaction can involve intermediates containing protonated apical oxygen intermediates also starting from the "cross" semidehydroxylated system (using CN1, CN2, and CN3 as CV). On the free energy surface (FES) we located three minima, initial (cross-semidehydroxylate with water), intermediate, and product (pyrophyllite). In the potential energy surface (PES) at 0 K, explored by optimization of the critical points along the MD trajectory, the free energy barrier between intermediate and final product, observed above in the FES, vanishes in the PES at 0 K indicating that the intermediate step is stabilized by entropic effects, as in the former case. Observing the evolution of the CVs in time (Figure 7a), we could match

**TABLE 1: Free Energy Barriers (kcal/mol) for the Reaction Paths**

| on-site semidehydroxylate | 900 K | 1500 K |
|---|---|---|
| pyrophyllite dehydroxylation[a] | 49.9[b] | 45.8[b] |
| rehydroxylation | 13.1[b], 19.3[c] | 7.4[b], 10.7[c] |
| second dehydroxylation | 30.9[a,b] | 29.0[a,b] |
| redroxylation-interconversion | 34.1 | |
| **cross semidehydroxylate** | **900 K** | **1500 K** |
| pyrophyllite dehydroxylation[a] | 48.3[b] | 38.7[b], 44.0[c] |
| rehydroxylation | 10.9[b], 3.5[c] | 1.5[c] |
| second dehydroxylation | 21.2[c] | 11.3[b] |
| redroxylation-interconversion | 20.2 | 11.0 |

[a] Previous results included for comparison.[12] [b] Direct mechanism. [c] With the assistance of the apical O atoms.

exactly the trajectory frames of each of these critical points, as well as the variation of the CVs at the point where the reaction takes place. Initially, we can observe the high value of CN2 of the cross-semidehydroxylate that decreases abruptly in the formation of the TS (increase of CN3) and the pyrophyllite (increase of CN1). For the rehydroxylation reaction, we estimated free energy barriers of 3.5 and 1.5 kcal/mol at 900 and 1500 K, respectively (Table 1). These values are significantly lower than that previously reported for the dehydroxylation reaction (44 kcal/mol at 1500 K)[12] and comparable with kT, indicating that this semidehydroxylate is unstable at high *T*. The protonation of the apical oxygen via the deprotonation of the water molecule involves crossing a potential energy barrier (activation energy) of 11.25 kcal/mol at 0 K (Figure 7b). This activation energy is similar to the one that we estimated before in the direct rehydroxylation mechanism (Figure 3). Hence, both mechanisms are likely to occur, but at high temperature the mechanism assisted by apical oxygens is favored (entropy should be higher, since at 900 K free energy is of 3.5 kcal/mol in the mechanism assisted by apical oxygen compared to 10.9 kcal/mol in the direct mechanism, Table 1).

All these rehydroxylation mechanisms showed in general lower activation energy at 0 K than the dehydroxylation reaction (Table 2). Our simulations have detected also a lower free energy barrier for the reaction path than that estimated from the energy profile of the dehydroxylation path obtained previously.[12] Therefore at high temperature, the rehydroxylation of the hydrated semidehydroxylate derivate is rather favored in front of the dehydroxylation reaction especially by the mechanism assisted by apical oxygens. In terms of free energy, the dehydroxylation reaction should be a combination of dehydroxylation−rehydroxylation reaction in agreement with the conclusions of previous experimental studies.[4,32]

**Rehydroxylation of the Fully Dehydroxylated Derivative. *Formation of the Dehydroxylate Pyrophyllite.*** The balance between dehydroxylation and rehydroxylation discussed above indicates that it is necessary to eliminate the water trapped in the tetrahedral cavity for progressing the reaction to the formation of the complete dehydroxylate derivative. This release of water is exothermic for the hydrated on-site semidehydroxylate ($\Delta E$ ) −20.6 kcal/mol), whereas is almost isothermic for the hydrated cross semidehydroxylate ($\Delta E$ ) −1.6 kcal/mol) (Table 2). In a previous work,[12] we found that the formation of the complete dehydroxylate derivative of pyrophyllite from the dry on-site semidehydroxylate intermediate requires similar activation energy (60.3 kcal/mol) that the initial partial dehydroxylation of pyrophyllite (59.7 kcal/mol). However, the free energy of formation of the on-site dehydroxylate was even lower

**TABLE 2: Energies of Reactant, Intermediates and Transition States of the Rehydroxylation Reactions of Pyrophyllite (At 0 K) Optimized**

| structures | energy (Hartrees) | $\Delta E$ (kcal/mol)[a] |
|---|---|---|
| (0) water | − 17.14342 | |
| (1) pyrophyllite intermediates | −426.91185 | |
| (2) on-site semidehydroxylate with water | −426.85029 | −38.6 (1-2) |
| | | −20.6 (4+0-2) |
| (3) cross semidehydroxylate with water | −426.83568 | −47.8 (1-3) |
| | | −1.6 (5+0-3) |
| (4) on-site semidehydroxylate without water | −409.73976 | |
| (5) cross semidehydroxylate without water | −409.69489 | 41.2 (5-4) |
| (6) first intermediate protonated in apical oxygen for on-site mechanism | −426.80158 | −69.2 (1-6) |
| | | 30.6 (6-2) |
| (7) first intermediate protonated in apical oxygen for cross mechanism | −426.84643 | −41.0 (1-7) |
| | | 28.1 (7-6) |
| | | 2.4 (7-2) |
| Transition States (TS) | | |
| (8) on-site direct mechanism | −426.81665 | 21.1 (8-2) |
| (9) cross direct mechanism | −426.81807 | 11 (9-3) |
| (10) on-site with assistance of apical oxygen | − 426.81412 | 22.7 (10-2) |
| (11) cross with assistance of apical oxygen | −426.81735 | 11.5 (11-3) |

[a] Energy differences between the structures numbered in the first column, whose numbers are in brackets.

than that of the first step (formation of semidehydroxylate). On the other hand, Guggenheim et al.[6] suggested that a higher energy is required for this second step of dehydroxylation than for the first step. To address this discrepancy, we first investigate the formation of the dehydroxylate through the cross mechanism.

Starting from the dry cross-semidehydroxylate intermediate without the trapped water molecule in the tetrahedral cavity we observed the dehydroxylation reaction at 900 K with the assistance of the tetrahedral apical O atoms with a free energy barrier of 21.2 kcal/mol. At 1500 K, a direct path of the dehydroxylation was obtained with a free energy barrier of 11.3 kcal/mol. In both cases, the same final product was obtained: the completely dehydroxylated derivative with a water molecule trapped in one tetrahedral cavity per unit cell. At 0 K, the activation energies were 29.9 and 15.5 kcal/mol for the path with apical oxygens assistance and direct way, respectively (Figure 8a,b). Both the free energy barrier and activation energy of the cross mechanism are lower than those of the on-site mechanism in the formation of the dehydroxylate derivative obtained previously.[12] Therefore, we can conclude that the free energy barriers at 900 and 1500 K and the activation energies at 0 K of the dehydroxylation of the semidehydroxylate intermediate (second step of dehydroxylation) are lower than those of the formation of semidehydroxylate intermediate (first step, formation of the first water molecule per unit cell) for all mechanisms investigated (on-site, cross, direct, and with apical oxygens assistance). However, in our simulations other paths were found that add further degrees of complexity to the process, as described below.

***Interconversion between Intermediates.*** In a continuation of the metadynamics run described above, using CN3 and D2 as CVs, we observed the interconversion of the dehydrated cross semidehydroxylated intermediate into the on-site semidehydroxylate (Figure 9a-c). At first, the OH changes its orientation (Figure 9a,b) and second the $AlO_rHAl$ group donates its proton to the $AlO_r(OH)Al$ group that is in front of it crossing the octahedral vacancy (Figure 9b,c). In this case, we estimated a free energy barrier of 20.2 and 11.0 kcal/mol at 900 and 1500 K, respectively. Again, these barriers are similar to those involved in the full dehydroxylation of the dehydrated semi-

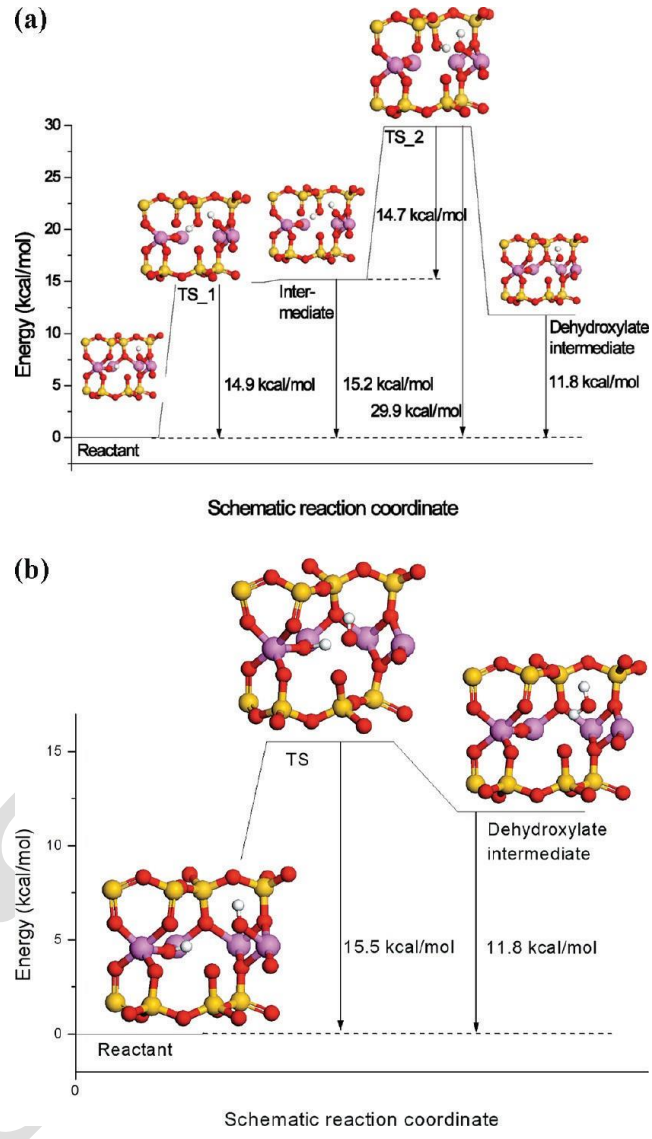


**Figure 8.** Reaction pathway at 0 K of the formation of the fully dehydroxylated derivative through the assistance of the apical O atoms (a) and through direct cross-way (b). H, Al, Si, and O atoms are in white, pink, yellow, and red colors, respectively.

dehydroxylate through the cross mechanism (21.2 kcal/mol at 900 K, and 11.3 kcal/mol at 1500 K) shown above. Hence the interconversion between intermediates effectively competes with dehydroxylation (Table 1).

The interconversion process is reversible, as proven by a simulation started from the dehydrated on-site semidehydroxylate intermediate with CN3 and D1 as CVs, although the mechanism is different. This interconversion takes place through a dehydroxylation of the on-site semidehydroxylate (Figure 10a,b) followed by a rehydroxylation (Figure 10b,c). This last step consists of a deprotonation of the water molecule previously formed and subsequent protonation of the residual oxygen (Or) in the neighboring cell yielding the cross semidehydroxylate. The free energy barriers are higher for the interconversion in this direction (34.1 kcal/mol at 900 K) than in the reverse way, but similar to that of the second dehydroxylation process of the on-site semidehydroxylate (30.9 kcal/mol[12]).

The interconversion from on-site to cross intermediates is thermodynamically less favored than that from cross to on-site intermediates due to the higher stability of the on-site intermediate with respect to the cross one (Table 2). On the contrary, the

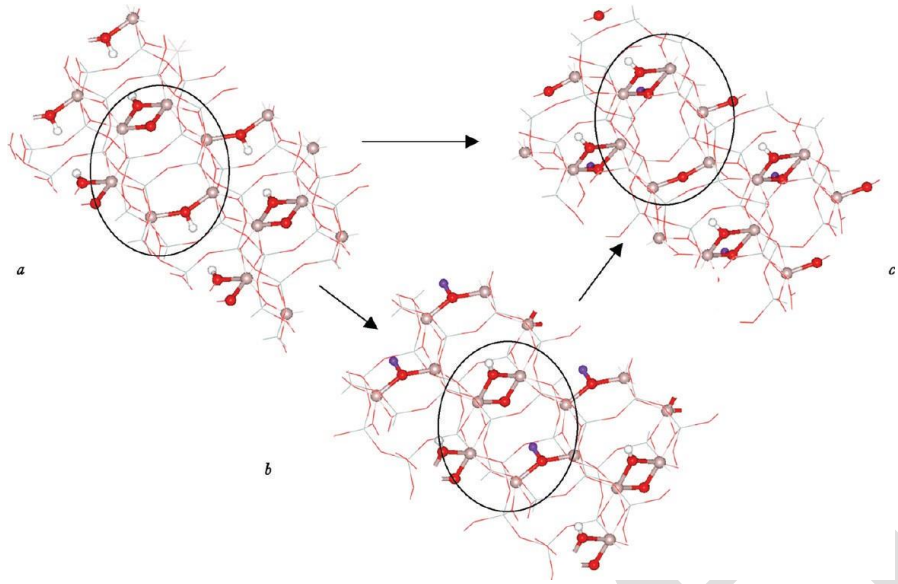


**Figure 9.** Interconversion between intermediates from cross one to the on-site one. Starting from the cross semidehydroxylate intermediate without water (a), OH groups change their orientation (b), and protonate the adjacent AlO(OH)Al group forming the on-site semidehydroxylate intermediate (c). The reaction centers are highlighted with spheres. View in 2 × 2 × 1 supercell from the (001) plane. H, Al, Si, H(Or), and O atoms are in white, pink, gray, blue, and red colors, respectively.

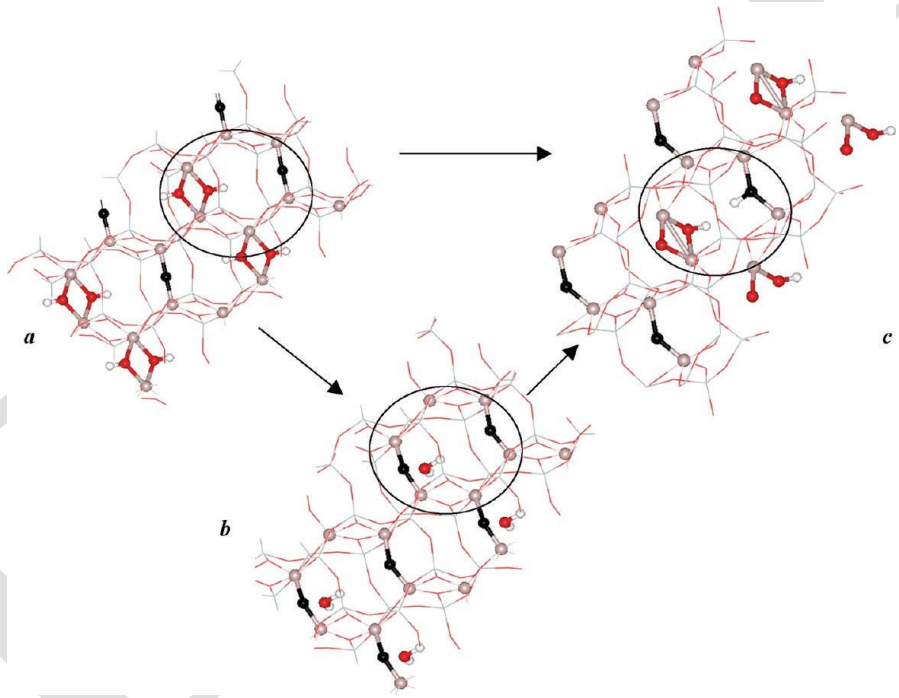


**Figure 10.** Interconversion between intermediates from the on-site one to the cross one. Starting from the on-site semidehydroxylate intermediate without water (a), the water is formed by dehydroxylation (b), and a further rehydroxylation produces the cross semidehydroxylate intermediate structure (c). The reaction centers are highlighted with spheres. View in 2 × 2 × 1 supercell from the (001) plane. H, Al, Si, Or, and O atoms are in white, pink, gray, black, and red colors, respectively.

cross intermediates should guarantee the progress of the dehydroxylation reaction by the cross mechanism, which is more likely to occur at high temperatures.[12] This is supported by the fact that the cross mechanism favors the second dehydroxylation at high temperature ($\Delta F$ ) 11.3 kcal/mol, with respect to the on-site mechanism, $\Delta F$ ) 29.0 kcal/mol at 1500 K). Furthermore, during metadynamics of the semidehydroxylates, either the second dehydroxylation or the interconversion into the other intermediate may occur in the same simulation (Figure 11 for the cross-semidehydroxylate). Therefore, we can identify the free energy surface for both processes at the same time, and estimate the free energy barriers. From up the reactant at the lowest energy point (large blue zones in Figure 11), reaction paths go ahead through the saddle points (transition states) to the intermediates (another energy minimum: protonated apical oxygen in case of dehydroxylation, to the left side of Figure 11a,b, or in case of interconversion in the right side of Figure 11a,b) and subsequently or directly to the products at a higher energy point: dehydroxylate with water formation (on the left side from the reactant of Figure 11a,b; lower values of D2 than in the reactant) or the interconverted semidehydroxylate (through an intermediate with one apical oxygen protonated, on the right

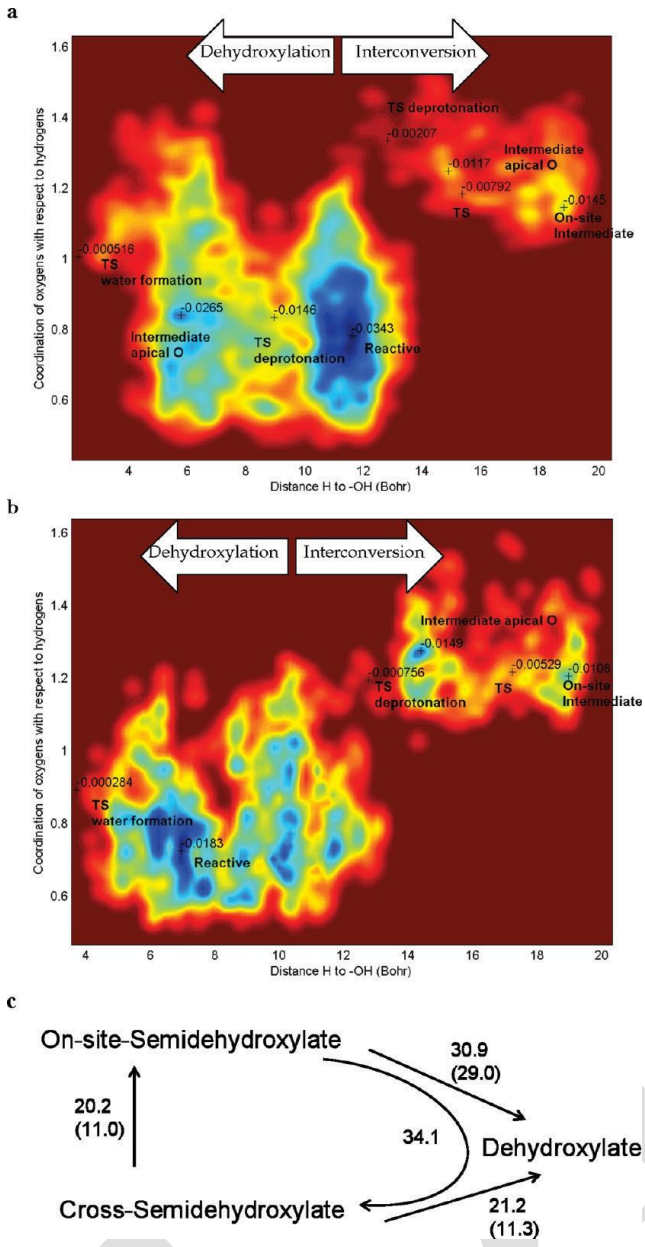


**Figure 11.** Free energy surface (CN3 vs D2) of the dehydroxylation reaction mechanism of the cross semidehydroxylate at 900 K (a) and at 1500 K (b). The reaction can evolve either to dehydroxylation (on the left) or to interconversion into the on-site intermediate (on the right). Free energy (Hartrees) varies from dark red at the maximum energy onto blue at the minimum energy. (c) Scheme of the dehydroxylation-rehydroxylation-interconversion reactions of the semidehydroxylate intermediates. The free energy barriers are included in kcal/mol at 900 K (values in brackets are at 1500 K).

side of Figure 11a,b; higher values of D2 than in the reactant), whichever come first. These results confirm us that the intermediate interconversion might inhibit or delay the progression of dehydroxylation by this mechanism at high temperature (Table 1).

## Conclusion

The present study suggests that the dehydroxylation of phyllosilicates at high temperatures is a combination of dehydroxylation and rehydroxylation reactions. Both reactions follow similar reversible reaction paths with two possible different mechanisms, the on-site one and the cross one. These processes may take place directly (in one step), or be assisted by apical oxygens (in two steps). The intermediates generated in the formation of the water molecule, the on-site and cross semihydroxylates, serve by themselves as reactants for the rehydroxylation reaction.

From our observations, the semidehydroxylates derivatives are rather unstable, since rehydroxylation is enormously facilitated. Moreover, the water molecule remains only during a short time scale in the octahedral hole by interacting with the apical oxygens. At this point, either it evolves rapidly to the initial structure by rehydroxylation, or it can either regenerate the opposite semidehydroxylate structure by interconversion between intermediates (cross to on-site or on-site to cross), or the water molecules can go out to the interlayer space and diffused out of the mineral. This latter second process is vastly favored at high temperature too.

Dehydroxylation and rehydroxylation processes compete also with interconversion between semidehydroxylates. As a consequence, the dehydroxylation reaction is hindered and requires more energy for further progressing. This provides an alternative explanation of experiment to that reported by Guggenheim et al.[6] The second step of the dehydroxylation does not have a higher activation energy than the first step, however the complete progress of the reaction is hampered by the competition between the dehydroxylation, rehydroxylation, and intermediate exchange processes. Within the equilibrium in the water-mineral system, the evaporation of water makes a shift of the equilibrium toward the formation of the dehydroxylate derivatives avoiding the rehydroxylation and the intermediates exchange. However, a further expose of moisture on the dehydroxylate derivatives will yield the rehydroxylation even at high temperatures.

These facts can justify the difficulty of identifying experimentally the dehydroxylation intermediates and may determine the rate limiting step of the dehydroxylation. This behavior can be extended at the least to the rest of dioctahedral 2:1 phyllosilicates.

**Acknowledgment.** We acknowledge support and useful discussions with Prof. Michele Parrinello. Authors are thankful to the Centro Te´cnico de Informa´tica of CSIC, centro de Ca´lculo del CIEMAT, Centro de Ca´lculo de Galicia (CESGA), and the Centro de Supercomputacio´n de la Universidad de Granada (UGRGRID) for allowing the use of its computational facilities. E.M.-M. is thankful to MEC for financial support within the FPU programme. This work was supported by Spanish MCYT and European FEDER Grants BTE2002-03838, CGL2005-02681, and CGL2008-06245-CO2-01.

## References and Notes

(1) Fitzgerald, J. J.; Dec, S. F.; Hamza, A. I. *Am. Mineral.* **1989**, *74*, 1405.
(2) Frost, R. L.; Barron, P. F. *J. Phys. Chem.* **1984**, *88*, 6206.
(3) Alvero, R.; Alba, M. D.; Castro, M. A.; Trillo, J. M. *J. Phys. Chem.* **1994**, *98*, 7848.
(4) Heller, L.; Farmer, V. C.; Mackenzie, R. C.; Mitchell, B. D.; Taylor, H. F. W. *Clay Miner. Bull.* **1962**, *5*, 56.
(5) Wang, L.; Zhang, M.; Redfern, S. A. T.; Zhang, Z. *Clays Clay Miner.* **2002**, *50*, 273.
(6) Guggenheim, S.; Chang, Y. H.; Van Groos, A. F. K. *Am. Mineral.* **1987**, *72*, 537.
(7) Drits, V.; Besson, G.; Muller, F. *Clays Clay Miner.* **1995**, *43*, 718.
(8) Mazzucato, E.; Artioli, G.; Gualtieri, A. *Phys. Chem. Miner.* **1999**, *26*, 375.
(9) Gualtieri, A. F.; Ferrari, S. *Phys. Chem. Miner.* **2006**, *33*, 490.
(10) Stackhouse, S.; Coveney, P. V.; Benoit, D. M. *J. Phys. Chem. B* **2004**, *108*, 9685.
(11) Sainz-D´ıaz, C. I.; Escamilla-Roa, E.; Herna´ndez-Laguna, A. *Am. Mineral.* **2004**, *89*, 1092.

(12) Molina-Montes, E.; Donadio, D.; Sainz-D´ıaz, C. I.; Herna´ndez-Laguna, A.; Parrinello, M. *J. Phys. Chem. B* **2008**, *112*, 7051.
(13) Molina-Montes, E.; Donadio, D.; Sainz-D´ıaz, C. I.; Herna´ndez-Laguna, A. *J. Phys. Chem. A* **2008**, *112*, 6373.
(14) Molina-Montes, E.; Timo´n, V.; Herna´ndez-Laguna, A.; Sainz-D´ıaz, C. I. *Geochim. Cosmochim. Acta* **2008**, *72*, 3929.
(15) Kloprogge, J. T.; Kamarneni, S.; Yanagirawa, K.; Fry, R.; Frost, R. L. *J. Colloid Interface Sci.* **1999**, *212*, 562.
(16) Car, R.; Parrinello, M. *Phys. Re*V. *Lett.* **1985**, *55*, 2471.
(17) *CPMD*, version 3.9.2.; IBM Corp., MPI fuer Festkoerperforschung Stuttgart: Stuttgart, 2004.
(18) Becke, A. D. *Phys. Re*V. *A* **1998**, *38*, 3098.
(19) Lee, C.; Yang, W.; Parr, G. M. *Phys. Re*V. *B* **1988**, *37*, 785.
(20) Troullier, N.; Martins, J. L. *Phys. Re*V. *B* **1991**, *43*, 1993.
(21) Lee, J. H.; Guggenheim, S. *Am. Mineral.* **1981**, *66*, 350.
(22) Kohn, W.; Sham, L. J. *Phys. Re*V. **1965**, *140*, 1133.
(23) Wardle, R.; Brindley, G. W. *Am. Mineral.* **1972**, *57*, 732.
(24) Laio, A.; Parrinello, M. *Proc. Nat. Acad. Sci. U.S.A.* **2002**, 12562.
(25) Iannuzzi, M.; Laio, A.; Parrinello, M. *Phys. Re*V. *Lett.* **2003**, *90*, 238.
(26) Churakov, S. V.; Iannuzzi, M.; Parrinello, M. *J. Phys. Chem. B.* **2004**, *108*, 11567.
(27) Laio, A.; Rodriguez-Fortea, A.; Gervasio, F.; Ceccarelli, M.; Parrinello, M. *J. Phys. Chem. B* **2005**, *109*, 6676. Laio, A.; Gervasio, F. L. *Rep. Prog. Phys.* **2008**, *71*, 126601.
(28) Bray, H. J.; Redfern, S. A. T. *Mineral. Mag.* **2000**, *64*, 337.
(29) Billeter, S. R.; Curioni, A.; Andreoni, W. *Comput. Mater. Sci.* **2003**, *27*, 437.
(30) Ensing, B.; Laio, A.; Parrinello, M.; Klein, M. L. *J. Phys. Chem. B* **2005**, *190*, 6676.
(31) Laio, A.; Parrinello, M. *Lect. Notes Phys.* **2006**, *703*, 315.
(32) Heller-Kallai, L.; Rozenson, lI. *Clays Clay Miner.* **1980**, *28*, 355.

JP102239K